



Article

Identification of New Purpuroine Analogues from the Arctic Echinodermata *Pteraster militaris* That Inhibit FLT3-ITD⁺ AML Cell Lines

Sara Ullsten ^{1,*} , Guillaume A. Petit ¹ , Johan Isaksson ^{2,3} , Ida K. Ø. Hansen ⁴ , Yannik K.-H. Schneider ¹ , Marte Jenssen ¹ , Chun Li ¹ and Kine Ø. Hansen ¹

¹ Marbio, UiT—The Arctic University of Norway, N-9037 Tromsø, Norway

² Department of Chemistry, UiT—The Arctic University of Norway, N-9037 Tromsø, Norway

³ Department of Pharmacy, Faculty of Health Sciences, UiT—The Arctic University of Norway, N-9037 Tromsø, Norway

⁴ Norwegian College of Fishery Science, Faculty of Biosciences, Fisheries and Economics, UiT—The Arctic University of Norway, N-9037 Tromsø, Norway

* Correspondence: sara.m.ullsten-wahlund@uit.no; Tel.: +47-77-649-272

Abstract: Isolation of bioactive products from the marine environment is considered a very promising approach to identify new compounds that can be used for further drug development. In this work we have isolated three new compounds from the purpuroine family by mass-guided preparative HPLC; purpuroine K-M. These compounds were screened for antibacterial- and antifungal activity, antibiofilm formation and anti-cell proliferation activity. Additionally, apoptosis-, cell cycle-, kinase binding- and docking studies were performed to evaluate the mechanism-of-action. None of the compounds showed activity in antibacterial-, antibiofilm- or antifungal assays. However, one of the isolated compounds, purpuroine K, showed activity against two cell lines, MV-4-11 and MOLM-13, two AML cell lines both carrying the FLT3-ITD mutation. In MV-4-11 cells, purpuroine K was found to increase apoptosis and arrest cells cycle in G1/G0, which is a common feature of FLT3 inhibitors. Interactions between purpuroine K and the FLT3 wild type or FLT3 ITD mutant proteins could however not be elucidated in our kinase binding and docking studies. In conclusion, we have isolated three novel molecules, purpuroine K-M, one of which (purpuroine K) shows a potent activity against FLT3-ITD mutated AML cell lines, however, the molecular target(s) of purpuroine K still need to be further investigated.

Keywords: marine Echinodermata; *Pteraster militaris*; marine secondary metabolite; marine bioprospecting; structure elucidation; FLT3



Citation: Ullsten, S.; Petit, G.A.; Isaksson, J.; Hansen, I.K.Ø.; Schneider, Y.K.-H.; Jenssen, M.; Li, C.; Hansen, K.Ø. Identification of New Purpuroine Analogues from the Arctic Echinodermata *Pteraster militaris* That Inhibit FLT3-ITD⁺ AML Cell Lines. *Int. J. Mol. Sci.* **2022**, *23*, 15852. <https://doi.org/10.3390/ijms232415852>

Academic Editor: Simone Ronsisvalle

Received: 20 October 2022

Accepted: 5 December 2022

Published: 13 December 2022

Publisher's Note: MDPI stays neutral with regard to jurisdictional claims in published maps and institutional affiliations.



Copyright: © 2022 by the authors. Licensee MDPI, Basel, Switzerland. This article is an open access article distributed under the terms and conditions of the Creative Commons Attribution (CC BY) license (<https://creativecommons.org/licenses/by/4.0/>).

1. Introduction

Marine invertebrates are viewed as a highly valuable source of lead compounds with potential of being developed into new medicines [1,2]. The endured interest in these compounds lies in their structural diversity and complexity and their desirable pharmacological properties [3]. As part of our ongoing effort to discover new bioactive compounds from marine invertebrates, fractions of the Echinodermata *Pteraster militaris*, collected at Kvadehuken, Svalbard, showed activity against the human melanoma cell line A2058 and the human pathogenic bacterium *Streptococcus agalactiae*. Previously, the fatty acid content of *P. militaris*, collected in Balsfjorden, Norway has been investigated [4]. This is however, to the best of our knowledge, the first investigation into the secondary metabolite content of the species. Through UHPLC-MS analysis, three compounds were identified as potential candidates to be responsible for the observed bioactivity. Following isolation and structure elucidation, the compounds were identified as members of the purpuroine family.

Compounds belonging to the purpuroine group have previously been isolated from the marine sponges *Pseudoceratina crassa* [5] and *Iotrochota purpurea* [6]. The common chemical features of the reported purpuroines are an alpha-amino acid with a trimethylated nitrogen, which is attached to a halogenated benzene ring via a C₂H₃ or C₃H₅O linker. In the herein reported purpuroines, the carboxylic terminal is methylated. Compounds similar to the purpuroines have been isolated from sponges belonging to the Verongiida order, like nakirodin A [7], aplysamine 3 and 4 [8] and others [5,9–12]. Previously, only limited bioactivity testing of the purpuroines have been conducted. However, both antibiotic activity and protein kinase inhibition have been reported [6].

Feline McDonough Sarcoma like tyrosine kinase receptor 3 (FMS-like tyrosine kinase 3 or FLT3) is a large transmembrane protein part of the receptor tyrosine kinase family. Its structure is divided in an extracellular receptor domain, a transmembrane domain followed by a juxta membrane (JM) domain and a cytoplasmic kinase domain split in two parts [13–16]. The kinase domains of FLT3 are usually kept in an inactivated state by the JM domain but upon binding of the FLT3 ligand (FL) to the receptor domain, FLT3 dimerize causing phosphorylation of tyrosine residues in the JM domain and activation loop, resulting in activation of the kinase domains [15]. Once active, FLT3 initiate multiple signal cascades including activation of the PI3K, AKT and RAS pathways and other tissues specific pathways leading to increases in cell proliferations and survival [17,18]. Mutations resulting in duplication of amino acid segments in the JM domain of FLT3, called internal tandem duplications (ITD), can lead to constitutive activation of the kinase, and of its downhill pathways [19]. FLT3 overactivation is the most common form of genetic alteration in acute myeloid leukemia (AML). While FLT3 inhibitors are clinically available, all come with serious adverse effects, including severe cardiac and hematological conditions [20].

The present study resulted in the isolation of three, previously not described, compounds belonging to the purpuroine family (Figure 1): purpuroine K (1), purpuroine L (2) and purpuroine M (3). Due to the previously reported bioactivity of the purpuroine family, the compounds were selected for further antibacterial and antiproliferative activity screening. Compound 1 showed selective inhibitory activity against FLT3 driven cancer cell lines. However, it did not display any direct binding to the active site of the kinase FLT3.

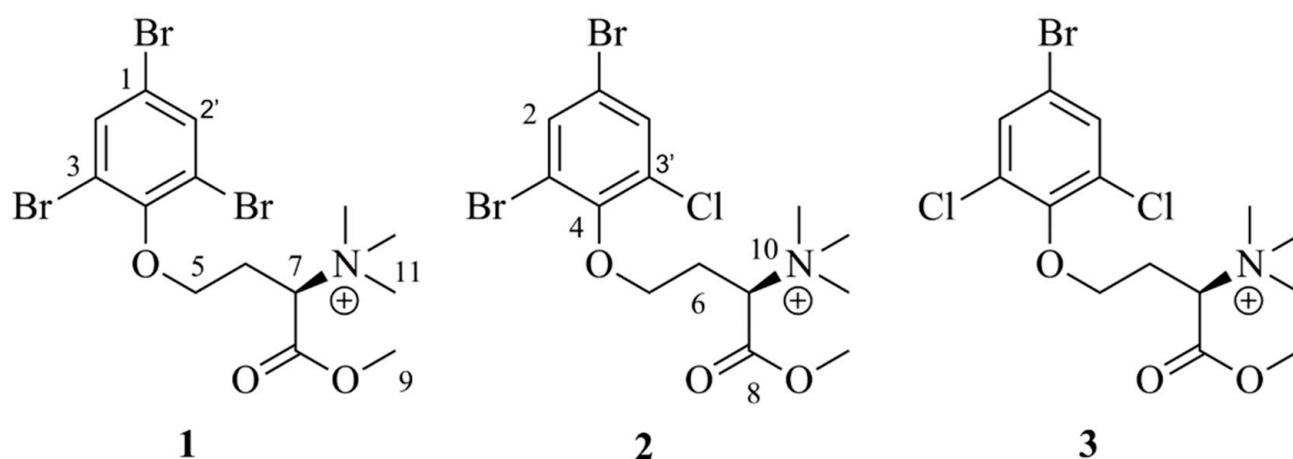


Figure 1. Structures of purpuroine K–M (compound 1–3) isolated as part of this work.

2. Results and Discussion

2.1. Biomass Collection, Extraction and Fractionation

Pteraster militaris was collected with a triangular bottom scrape off the coast of Kvadehuken, Spitzbergen (78°57'58" N, 11°19'41" E, wet weight = 2440.8 g). The sample was freeze-dried (dry weight = 391.3 g) and extracted with MQ-water. The resulting pellet (dry weight = 278.9 g) was re-dried and extracted twice in MeOH:CH₂Cl₂ (1:1). After filtration,

the solvent was evaporated under reduced pressure, yielding the organic extract (43.5 g). The organic extract was fractionated into eight fractions using RP flash chromatography.

2.2. Viability and Antibacterial Screening of the Flash Fractions

The flash fractions of *P. militaris* were assayed for activity against the human melanoma cancer cell line A2058 at 50 µg/mL. For fraction five, this resulted in 23% cell survival. The flash fractions were also assayed against the human pathogenic bacterial strains *Staphylococcus aureus*, *Enterococcus faecalis*, *Escherichia coli*, *Pseudomonas aeruginosa* and *Streptococcus agalactiae* (Gr. B). Flash fractions three, four and five were found to be active against *Streptococcus agalactiae* at a concentration of 250 µg/mL.

2.3. Dereplication of the Active Fractions

To identify the compound(s) responsible for the activity against the A2058 cell line, the active fraction five as well as the inactive fractions four and six were analyzed using UHPLC-HR-MS (Figure 2). In the chromatogram for fraction five, three halogenated secondary metabolites stood out. Their elemental compositions were calculated to be $C_{14}H_{19}NO_3Br_3$ (1), $C_{14}H_{19}NO_3ClBr_2$ (2) and $C_{14}H_{19}NO_3Cl_2Br$ (3).

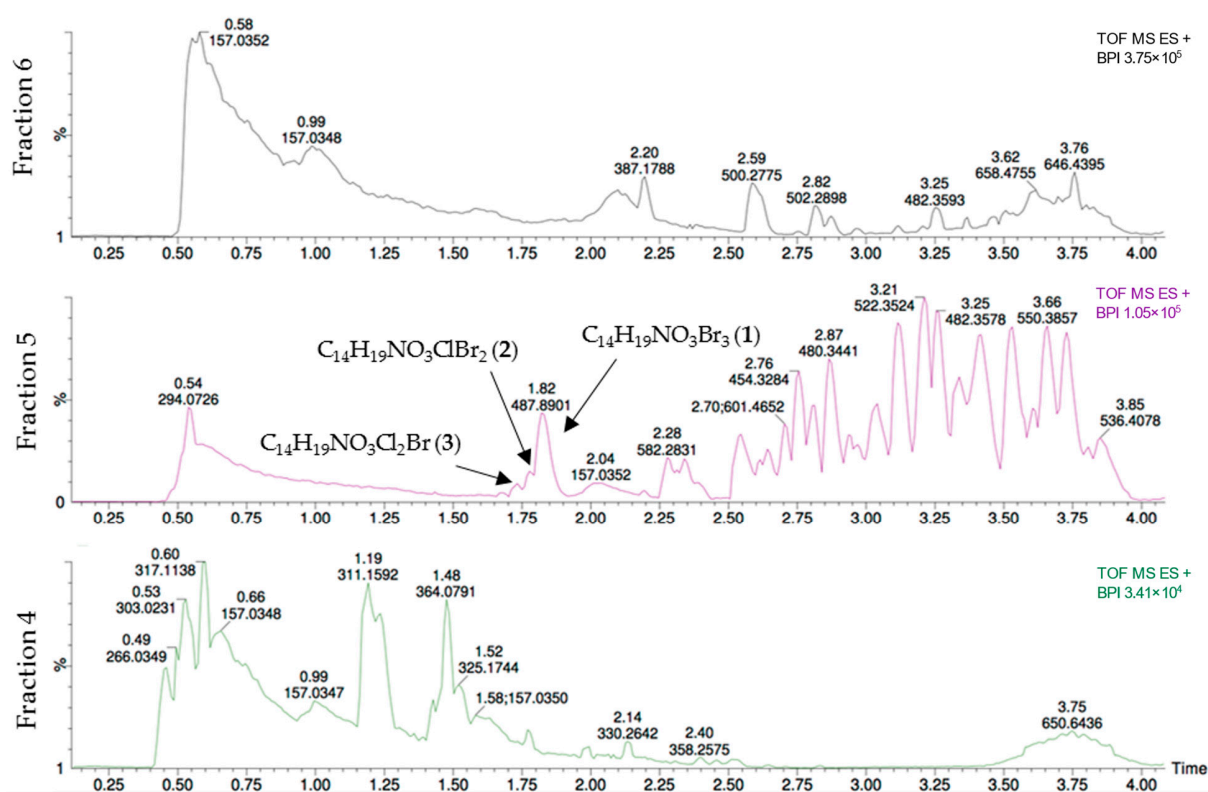


Figure 2. UHPLC-HR-MS chromatograms of the cytotoxic flash fraction five, as well as the non-cytotoxic fractions four and six of the organic extract of *Pteraster militaris*. Three halogenated secondary metabolites were exclusively present in flash fraction five, which suggests their involvement in the activity seen towards the human melanoma cell line A2058.

The elemental compositions did not yield any hits when used as input in compound databases. As these compounds only are present in fraction five, they are likely candidates to be the compound causing the activity against the A2058 melanoma cell line and were therefore selected for isolation. In a similar manner, the chromatograms for fractions three to five were compared to fractions two and six to identify the compound(s) responsible for the antibacterial activity. In this analysis, no compound was found to be present only in the antibacterial fractions. It is possible that compounds 1–3 are responsible for the antibacterial

activity observed for fraction five, while different compounds are responsible for the activity displayed for fractions four and three. Based on the dereplication of the fraction displaying antibacterial activity, no additional compounds were nominated for isolation.

2.4. Isolation of 1–3

Compound 1–3 were isolated from 4.06 g of the organic extract of *P. militaris* using mass guided semi-preparative HPLC. Stepwise purification using RP HPLC columns with phenyl-hexyl and C18 packing material led to the isolation of three novel purpuroine variants: purpuroine K (1) (4.3 mg), purpuroine L (2) (1.1 mg) and purpuroine M (3) (0.7 mg).

2.5. Structure Elucidation of 1–3

Purpuroine K (1) was isolated as a light-yellow wax. HRESIMS analyses supported an elemental composition of $C_{14}H_{19}Br_3NO_3$ (m/z 486.8996 $[M + H]^+$, calculated 486.8993), requiring five degrees of unsaturation. 1H and ^{13}C NMR analysis (Tables 1 and 2, Figures S1–S5) confirms the presence of 16 hydrogens and 14 carbons. 1D and 2D NMR analysis recorded for 1 revealed high structural similarity to purpuroine A (4) [6], with the addition of a H_3 signal (H_3-9) at 3.83 ppm (Figure S1) and a primary carbon (C-9) signal at 53.7 ppm (Figure S2). Through a HMBC correlation between H_3-9 ($\delta_H = 3.83$) and C-8 ($\delta_C = 167.2$), the additional methyl group of 1 compared to 4 could be placed at the hydroxyl oxygen of the carboxylic acid functionality of 4. The remaining 1D and 2D NMR data corresponded well for that recorded for 4 (Tables S1 and S2). Key COSY and HMBC correlations can be seen in Figure 3. The halogenation pattern of the benzene ring was confirmed through HSQC correlations between H-2 ($\delta_H = 7.97$, 2 protons integral) and C-2 ($\delta_C = 134.0$) and the lack of HSQC correlations to C-1 ($\delta_C = 117.9$) and the two NMR equivalent C-3 ($\delta_C = 118.6$) carbon atoms. The deshielded ppm of C-4 ($\delta_C = 151.9$) confirms that the rest of the molecule is linked to this carbon via an oxygen atom. Compound 1 has one stereocenter at C-7. All the previously reported purpuroines and other N-trimethyl-D-homoserine derivatives have an S-configuration in this stereocenter (initially reported as R5, but later confirmed to be S through synthesis [21]). They also all show positive signs of specific rotation. The measured $[\alpha]_D^{20} +13.63 \pm 0.02$ of 1 therefore indicates the absolute configuration of C-7 to be S.

Table 1. 1H -NMR spectroscopic data (600 MHz, DMSO- d_6) for purpuroines K–M (1–3).

Position	δ_H , m (J in Hz)		
	1	2	3
2		7.87, d (2.3)	7.84, s
2'	7.97, s	7.94, d (2.3)	
5a			4.09–4.04, m
5b	4.01, m	4.08–3.95, m	4.02–3.95, m
6a	2.74, m	2.76–2.68, m	2.71, s
6b	2.42, m	2.42, t (6.3)	2.42, d (8.0)
7	4.59, d (11.0)	4.55, dd (11.7, 2.5)	4.59–4.52, m
9	3.83, s	3.83, s	3.82, s
11	3.27, s	3.24, s	3.24, d (3.1)

Table 2. ^{13}C -NMR spectroscopic data (150 MHz, DMSO- d_6) for purpuroines K–M (1–3).

Position	δ_C , Type		
	1	2	3
1	117.9, C	117.5, C	117.0, C
2		132.3, CH	131.7, CH
2'	135.0, CH	134.4, CH	
3		118.9, C	129.5, C
3'	118.6, C	129.2, C	
4	151.9, C	150.9, C	149.9, C

Table 2. Cont.

Position	δ_C , Type		
	1	2	3
5	69.0, CH ₂	69.1, CH ₂	69.2, CH ₂
6	27.3, CH ₂	27.3, CH ₂	27.2, CH ₂
7	71.0, CH	71.1, CH	71.1, CH
8	167.2, C	167.2, C	167.2, C
9	53.7, CH ₃	53.6, CH ₃	53.6, CH ₃
11	51.7, CH ₃	51.7, CH ₃	51.7, CH ₃

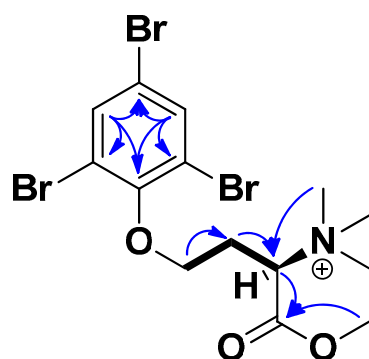


Figure 3. Key COSY (bold) and HMBC (blue arrows) correlations of purpuroine K (1).

Purpuroine L (2) was isolated as a light brown wax. HRESIMS analyses supported an elemental composition of C₁₄H₁₉Br₂ClNO₃ (m/z 442.9414 [M + H]⁺, calculated 442.9499), requiring five degrees of unsaturation. Purpuroine M (3) was isolated as a light brown wax. HRESIMS analyses supported an elemental composition of C₁₄H₁₉BrCl₂NO₃ (m/z 398.9953 [M + H]⁺, calculated 399.0004), requiring five degrees of unsaturation. The ¹H and ¹³C NMR analysis (Tables 1 and 2, Figures S6–S15) of 2 and 3 showed close structural similarity to 1 and 4. The core structures of 2 and 3 was solved in a similar manner as above mentioned for 1. Compounds 2 and 3 thus have the same purpuroine backbone as 1. When comparing the elemental compositions of 2 and 3 to the elemental composition of 1, 2 has exchanged one bromine atom for a chlorine atom and compound 3 has exchanged two bromine atoms for chlorine atoms. For 2, the chlorine atom was placed on C-3' ($\delta_C = 129.2$) due to the downfield shift value of this carbon atom compared to the brominated carbon atoms of compound 1 (C-1: $\delta_C = 117.9$, C-3/C-3': 118.6) and the brominated carbon atoms of 2 (C-1: $\delta_C = 117.5$, C-3: $\delta_C = 118.9$). For 3, the downfield shift value of C-3 and C-3' (both $\delta_C = 129.5$) compared to C-3 and C-3' of 1 (both $\delta_C = 118.6$), places the chlorine atoms in these positions.

All the previously isolated purpuroine variants had an unmethylated carboxylic group in common. Their originating biomass, the sponge *I. purpurea*, was extracted with- and analyzed in MeOH [6]. Furthermore, sample preparation of similar compounds, like nikirodin A (with an unmethylated carboxylic acid terminal) also involved solving the biomass in methanol [7]. This indicates that the herein isolated compounds are not methylated by the extraction solvent creating artifacts of the previously reported purpuroine A, E and C, which are the unmethylated carboxylic acids of the corresponding methyl esters 1, 2 and 3, respectively. The sample of *P. militaris* did not contain traces of unmethylated variants of 1–3.

2.6. Benefits to *P. militaris* and the Proposed Biosynthetic Origin of 1–3

The concentrations of compounds 1–3 were 18.88, 4.83 and 3.074 mg/kg wet weight *P. militaris*, respectively. These high concentrations indicate that they have beneficial effects for *P. militaris*. As part of this work, 1 has been shown to be cytotoxic. *P. militaris* may thus use the compounds as a defense strategy to deter predators. Some marine species have been reported to ingest organisms and sequester their secondary metabolites, using

them as a chemical defense against pathogens or predators [22,23]. Species belonging to the *Pteraster* genus have been shown to primarily feed on sponges, and the herein isolated purpuroines may thus stem from a dietary source of *P. militaris* [24,25]. This is known as an acquired chemical defense strategy. As the purpuroines have been reported from sponge species that are only remotely related (*I. purpurea* and *P. crassa* belong to the same class; Demospongiae), the producer of the purpuroines may furthermore be microorganisms living in symbiosis with the sponges. The biosynthetic origin of the purpuroines remains to be determined.

2.7. Antifungal, Antibacterial and Biofilm Formation Inhibiting Activity of 1–3

Due to previous documentation of antibacterial activity of compounds from the purpuroine family, compounds 1–3 were tested in a broad antibacterial, antifungal and biofilm formation panel. The compounds were more specifically tested for growth inhibition of the *Candida albicans* (ATCC 10231) yeast and the mould strains *Rhodotrula* sp. and the *Aurobasidium pollulans*, five pathogenic bacterial strains, *S. aureus*, *E. coli*, *E. faecalis*, *P. aeruginosa* and *S. agalactiae*, and for inhibition of biofilm formation of *S. epidermidis*. In all assays the test concentrations of the compounds were 150 μ M. None of the compounds displayed activity against the microorganisms or against biofilm formation. As variants of 1 and 3 with an unmethylated carboxyl terminal previously have been reported as antifungal (IC₅₀ of around 27 μ M against *Aspergillus fumigatus*), this indicates that methylation of the carboxylic acid is detrimental to the antifungal activity. Furthermore, another closely related purpuroine variant (substituted at C-3 with bromine, at C-1 with hydrogen at C-5 with iodine and with a C₂H₄ linker and an unmethylated carboxylic acid terminal) has shown activity against *Streptococcus pneumoniae*.

While flash fractions three, four and five were found active against *S. agalactiae* at 250 μ g/mL, there were no indications that 1–3 had growth inhibiting activities or biofilm formation inhibiting activity against any of the test strains. This indicates that a different compound present in the flash fractions was responsible for the observed antibacterial activity against *S. agalactiae*, or that a mixture of compounds produced the observed antibacterial activity.

2.8. Viability Screening and IC₅₀ Determination of 1–3

Anti-viability activities of 1–3 were evaluated in a panel of normal and cancerous cell lines at 10 μ M and 50 μ M (Table 3). Flash fraction five was initially active against A2058 cells. However, the isolated compounds 1–3 from this fraction did not show activity towards this cell line. This indicates that we did not isolate the sample component responsible for the initial observed activity, or that synergistic effects among several sample components in flash fraction five caused the cytotoxic activity. When the compounds were further studied in our full viability screening panel, 2 and 3 did not show any activity against any of the cell lines tested. However, 1 did decrease the viability of the two AML derived cell lines MV-4-11 and MOLM-13. These two cell lines are both carrying an internal tandem duplication of FLT3 (FLT3-ITD). The mutation results in autophosphorylation and constitutive activation of the receptor and multiple proliferative and survival pathways [26] leading to enhanced cell division and survival. Compound 1 seems to selectively inhibit leukocyte cell lines driven by FLT3-ITD as other leukemia derived cell lines remained unaffected suggesting inhibition of the FLT3 kinase. The active compound 1 was selected for further IC₅₀ determination in the MV-4-11 cell line as well as apoptosis, cell cycle and kinase binding assays. IC₅₀ of 1 against MV-4-11 was determined to be 26 \pm 1.2 μ M. Due to the lack of activity, 2 and 3 were not selected for further cellular or kinase binding studies.

Table 3. Screening of cytotoxic effect of compound 1–3.

Cell Line	Cell Type	Activity at $\leq 50 \mu\text{M}$ ¹		
		1	2	3
MRC5	Lung fibroblasts (non-cancerous)	I ²	I	I
HaCat	Keratinocytes (non-cancerous)	I	I	I
SK-BR-3	Breast cancer	I	I	I
MDA-MB-468	Breast cancer	I	I	I
MV-4-11	Acute myeloid leukemia	Active	I	I
MOLT-4	Acute lymphoblastic leukemia	I	I	I
A2058	Melanoma	I	I	I
HT29	Colon cancer	I	I	I
HepG2	Liver hepatocellular carcinoma	I	I	I
MOLM-13	Acute myeloid leukemia	Active	I	I
THP-1	Acute monocytic leukemia	I	I	I

¹ The cytotoxic effect of compound 1–3 was evaluated in our in-house screening panel of cancerous and non-cancerous cell lines. Each compound was screened at 10 and 50 μM , active compound was defined as $\leq 50\%$ survival at one of the concentrations. All samples were run in triplicates. ² Inactive.

2.9. Cell Cycle Analysis

To further reveal how **1** inhibits the growth of MV-4-11 cells, cell cycle analysis was performed (Figure 4). After 24 h of stimulation with **1**, significant inhibition of the cell cycle was observed at 52 μM and 104 μM compound concentration, by causing an increase in the number of cells arrested in G0/G1 phase by 11% and 19%, respectively. Parallely a decrease of 23%, respectively, 38% of cells entering the S-phase was seen and a decrease of 26%, respectively, 55% of cells entering G2/M-phase was also observed. The progression of cells through, and exit from G0/G1, is regulated by cyclins and cyclin-dependent kinases (CDKs) [27]. Interestingly, the FLT3 kinase, which drives the proliferation of the MV-4-11 cell line, induces downstream activation of cyclin D2 and D3 which both activates CDK6 [28]. Inhibition of FLT3 has in previous studies resulted in downregulation of these cyclins which explains the common feature of G0/G1 arrest in MV-4-11 cells seen after treatment with FLT3 inhibitors [29,30].

2.10. Induction of Apoptosis

To further investigate the cell death pathway activated by **1**, an apoptosis assay was performed and the ability of **1** to induce apoptosis and/or necrosis in MV-4-11 cell line was evaluated by annexin V/PI staining (Figure 5). The cells were divided into 3 different populations: annexin V⁻/PI⁻ (healthy cells), annexin V⁺/PI⁻ (apoptotic cells) and annexin V⁺/PI⁺ (late apoptotic/necrotic cells). After 24 h incubation, the percentage of apoptotic cells after treatment with 26 μM **1** ($1 \times \text{IC}_{50}$) were almost doubled (94% increase) when compared to control (Figure 5a,c). The induction of apoptosis was both time- and dose-dependent indicating that the target of **1** is involved in the apoptosis signaling pathway. Interestingly, FLT3 inhibitors also induce apoptosis in MV-4-11 cells which further strengthen our hypothesis that **1** targets the FLT3 kinase [31–33]. However, after 24 h and 48 h of incubation at the highest concentration of compound (104 μM), no increase in apoptotic cells were seen when compared to cells incubated with 52 μM . At this concentration, late apoptotic/necrotic cells instead increased significantly (Figure 5a–c). High concentrations of compound **1** does thus seem to induce necrosis over apoptosis, suggesting that multiple different targets may be affected at this concentration which is a common profile of natural products [34].

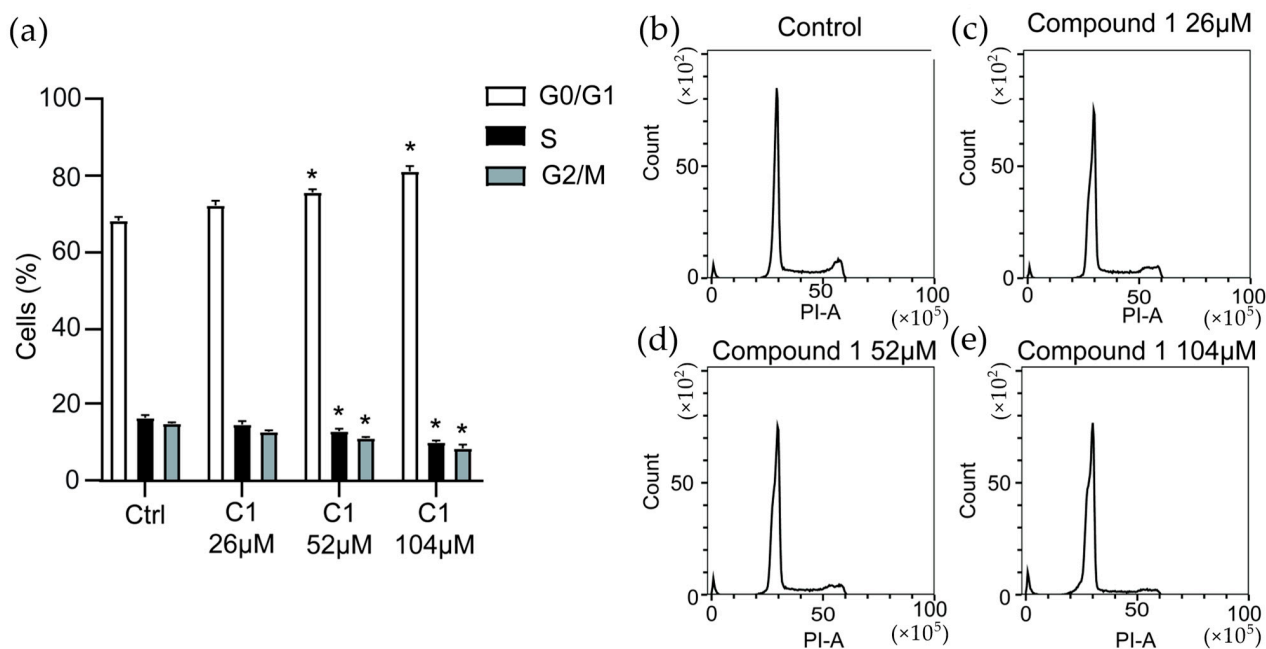


Figure 4. Cell cycle analysis. (a) MV-4-11 cells are significantly arrested in G0/G1 phase after treatment with 1 at 52 and 104 µM ($2 \times IC_{50}$ and $4 \times IC_{50}$, respectively) with a corresponding decrease in cells in S and G2/M phase when compared to control ($n = 3$). (b–e) representative images of flow cytometry data. * denotes $p \leq 0.05$.

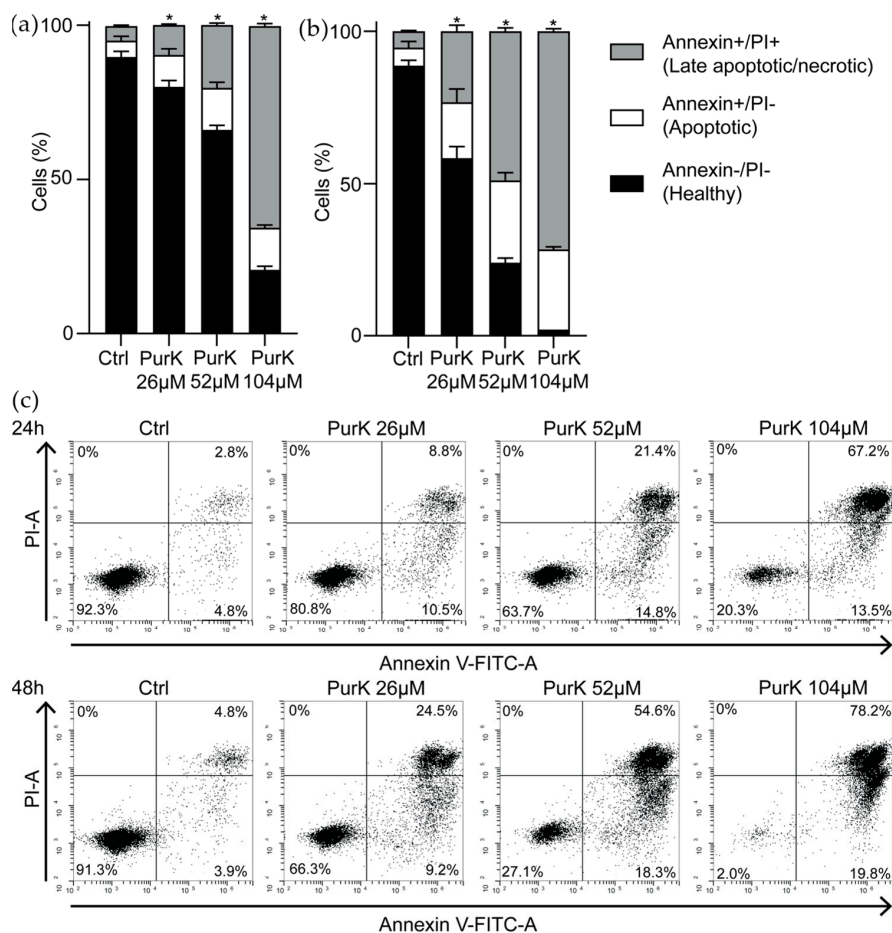


Figure 5. Apoptosis assay. Compound 1 (PurK) increased apoptosis in MV-4-11 cells after 24 h (a)

and 48 h (b) at 26 μM , 52 μM and 104 μM compound concentration ($1 \times \text{IC}_{50}$, $2 \times \text{IC}_{50}$ and $4 \times \text{IC}_{50}$, respectively) when compared to control ($n = 3$). At 104 μM of compound 1, the percentages of cells in late apoptotic/necrotic phase rather than apoptotic cells increased compared to the lower concentration of 52 μM , indicating induced toxicity or that multiple targets are being affected at this concentration. Representative flow cytometry images (c). * denotes $p \leq 0.05$.

2.11. Kinase Binding and Docking

The FLT3-ITD mutant kinase is known to promote proliferative and survival pathways within the MV-4-11 and MOLM-13 cell lines. Together with selective inhibition of these two cell lines, our testing also demonstrates that MV-4-11 cells tend to arrest in the G0/G1 phase and go through apoptotic cell death upon treatment with 1. These features are similar to FLT3 inhibitors [29,30]. In addition, some of the purpurines reported previously displayed activity against disease relevant kinases [6]. As a result, it was decided to test the binding affinity between 1 and two FLT3 variants, namely the FLT3 wild type (WT) and FLT3-ITD mutant.

In short, the binding between a compound of interest and the FLT3 active site can be measured with fluorescence resonance energy transfer (FRET). A FRET signal is generated between an Europium-labelled tag, on the FLT3 kinase, and a fluorescent tracer with high binding affinity for the FLT3 active site. During the assay, the compounds tested will compete against the tracer for the kinase active site, resulting in a decrease in the FRET signal based on the compound binding affinity for the kinase active site.

Compound 1 did not cause a decrease in the FRET signal in our experimental set up, at working concentration of up to 10 μM . Since the quizartinib control worked as expected, these results suggest that 1 does not bind to the active site pocket of the FLT3 variants tested (Figure 6).

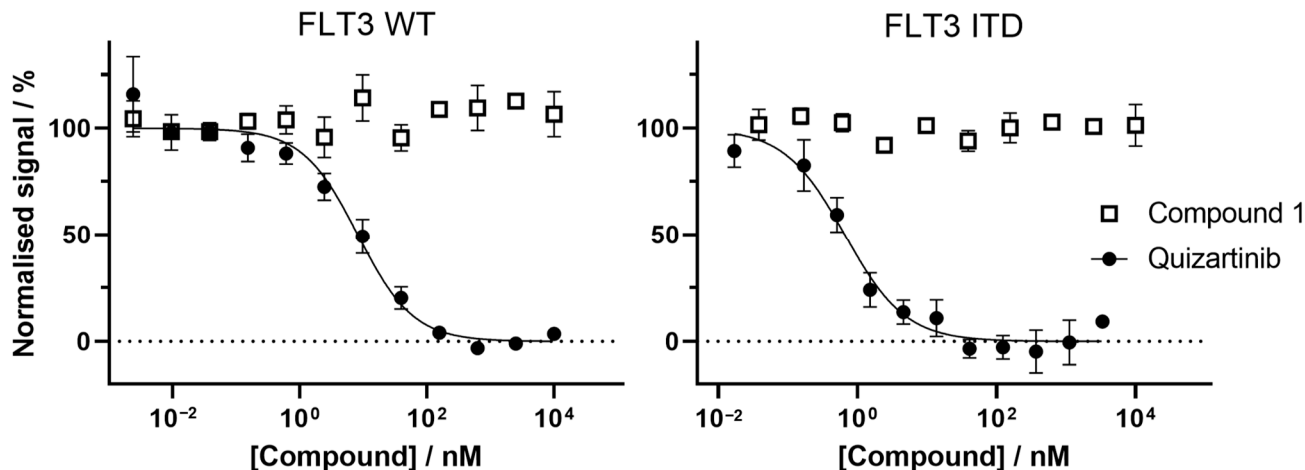


Figure 6. Measurement of binding between 1 and FLT3 variants. Compound 1 (squares) does not bind to either FLT3 WT or FLT3-ITD mutant active site at the concentrations tested (up to 10 μM). The emission ratio (normalized signal) remains constant despite increasing compound concentration. As a comparison, quizartinib (solid circles) behave as expected, with IC_{50} of 8.2 nM against FLT3 WT and 0.7 nM against FLT3-ITD mutant, calculated from fitting the normalized signal with an inhibitory dose response curve (see methods). Error bars represent the standard deviation ($n = 3$). The X-axis is the Log_{10} of the compound concentrations in nanomolar (nM), and the Y-axis shows the normalized emission ratio signal.

In parallel to measuring the binding affinity of compound 1 for FLT3, 1–3 were also computationally docked in the FLT3 WT kinase domain, using the crystallographic model with Protein DataBank (PDB) ID: 6JQR [35], to evaluate their potential binding modes. Several poses were identified for compounds 1 to 3 using Glide (Schrödinger LLC, release 2022-2) [36–38], however none of the poses were calculated to bind strongly to the active

site and no strong interaction with the ATP binding pocket of FLT3 was observed (Figure 7). As a validation of the method used, the endogenous FLT3 ligand gilteritinib, from the same crystal structure, was successfully docked back to its original position (Figure S16).

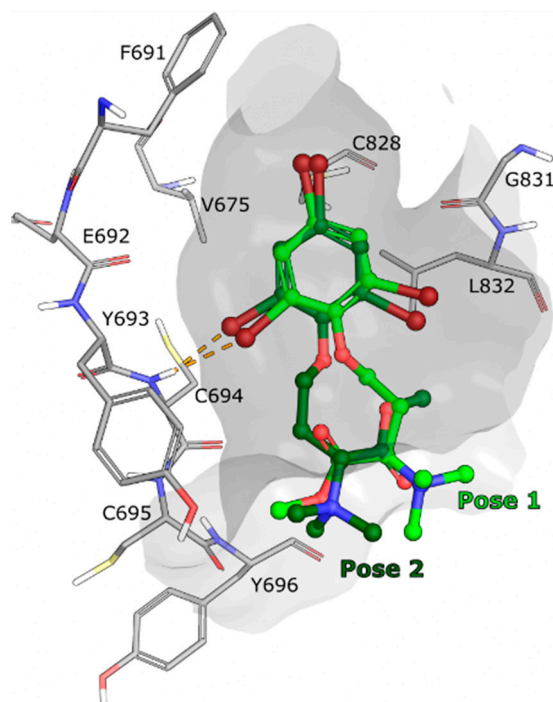


Figure 7. Docking of **1** in the active site of FLT3 WT model PDB ID: 6JQR [35]. Compound **1** is placed in the active site pocket (shown as a grey surface) in two different manners: pose 1 (light green carbon atoms) and pose 2 (dark green carbon atoms), with similar docking scores (both around -5.9 , suggesting weak binding). Pose 2 is roughly a 180-degree rotation of pose 1 along the long axis of the molecule. However, none of the poses suggest any specific interaction with FLT3 beyond having dimensions that roughly match its active site cavity. FLT3 residues that are in proximity of **1** are displayed as grey sticks and labelled. Color code for non-carbon atoms: hydrogen atoms are shown in white, nitrogen atoms in blue, oxygen atoms in red, sulfur atoms in yellow and bromine atoms in maroon. The orange dashed lines represent too-close contacts.

Based on the experimental binding affinity experiment and computational docking experiments, it is unlikely that compounds **1–3** are binding strongly to the active site of the FLT3 variants. There is however a possibility that **1** interacts with other parts of the FLT3 kinase, that would not directly affect the active site. For example, modulating the kinase activity by interacting with the activation loop, the JM domain or even potentially with the extracellular receptor domain of FLT3, which is not present in the binding assay (only the cytoplasmic domain is used). A kinase activity assay could determine whether **1** is regulating the activity of the kinase from an allosteric site. It is also possible that compound **1** is affecting another target located downstream of the FLT3 kinase which could generate similar phenotype as a FLT3 inhibitor. While the mode of action remains to be deconvoluted, this highlights the possibility of discovering a new and selective manner to target severe and aggressive FLT3-ITD driven AML.

3. Materials and Methods

3.1. General Experimental Procedures

Optical rotations were measured on an AA-10R automatic polarimeter (Optical activity LTD., Huntingdon, UK) in MeOH. NMR spectra were acquired in DMSO- d_6 on a Bruker Avance III HD (Bruker, Billerica, MA, USA) spectrometer operating at 600 MHz for protons, equipped with an inverse TCI cryo probe enhanced for ^1H , ^{13}C and ^2H . All NMR spectra

were acquired at 298 K, in 3 mm solvent matched Shigemi tubes using standard pulse programs for Proton, Carbon, HSQC, HMBC, DQCOSY and ROESY with gradient selection and adiabatic versions where applicable. $^1\text{H}/^{13}\text{C}$ chemical shifts were referenced to the residual solvent peak (DMSO- d_6 : $\delta_{\text{H}} = 2.50$, $\delta_{\text{C}} = 39.51$). HRESIMS were performed using a Waters LCT Premier Time-of-Flight MS with an Acquity UPLC (Waters, Milford, MA, USA), using MS grade solvents and a Waters Acquity UPLC BEH (1.7 μm , 2.1×100 mm) column. Compound isolation was performed using a preparative-HPLC-MS system consisting of a 600 HPLC Pump, a 2996 Photodiode Array UV detector, a 3100 Mass detector, and a 2767 sample manager (all from Waters). The following columns were used: Xselect CSH Phenyl-Hexyl Prep (5 μm , 10×250 mm) and SunFire. Flash chromatography was carried out using a Biotage HPFC SP4 system equipped (Biotage, Uppsala, Sweden) with a Biotage SNAP column filled with 8 g Diaion HP-20SS (Supelco Analytical, Merck, Darmstadt, Germany). All solvents used for extraction and fractionation were of HPLC grade and Milli-Q H_2O was used.

3.2. Biological Material

Individuals of the Echinodermata *Pteraster militaris* (class Asterozoa, order Velatida, family Pterasteridae) were collected with a triangular bottom scrape at Kvadehuken, Svalbard (78.9662° N, 11.3269° E) in 2011. The organism was identified by Robert A. Johansen, at the Norwegian national biobank (Marbank) and a voucher specimen (ref. M14064) was deposited in Marbank, Tromsø, Norway. The specimen was stored at -23 °C in the dark until processed.

3.3. Extraction and Flash Fractionation

Freeze-dried *P. militaris* (wet weight 2440.8 g) was diced and extracted twice with water at 4 °C in the dark. After supernatant removal, the remaining pellet was freeze-dried (dry weight: 391.3 g) and extracted twice in 50:50 MeOH:CH₂Cl₂ (vol:vol). After filtration, the solvent was pooled and evaporated under reduced pressure, and a dark red, oily residue (43.5 g) was obtained. An aliquot of the extract (1.53 g) was then fractionated using flash chromatography on a prepacked column filled with Dainon HP-20SS resin (8 g). The following step gradient was applied: MeOH/H₂O to MeOH in five steps (5:95, 25:75, 50:50, 75:25, 100:0) followed by MeOH:acetone to acetone in two steps (50:50, 0:100) with a flow rate of 12 mL/min. A total of eight fractions were collected (72 mL each) and dried under reduced pressure.

3.4. Antibacterial Screening of the Flash Fractions

The flash fractions of *P. militaris* were assayed for activity against the human pathogenic bacterial strains *Staphylococcus aureus* (ATCC 25923), *Enterococcus faecalis* (ATCC 29212), *Escherichia coli* (ATCC 25922), *Pseudomonas aeruginosa* (ATCC 27853) and *Streptococcus agalactiae* (Gr. B) (ATCC 12386) at a concentration of 250 $\mu\text{g}/\text{mL}$. Briefly, suspended bacteria in log phase were added to 96-well microtiterplates at a concentration of 1.500–15.000 colony forming units/mL. The flash fractions were subsequently added and left to inoculate for 24 h before growth inhibition was observed using a 1420 Multilabel Counter VICTOR3™ (Perkin Elmer, Waltham, MA, USA) at 600 nm. Growth medium diluted with water (1:1) was used as negative control, and bacteria suspension diluted with water (1:1) as positive control. Gentamycin was used as positive assay control.

3.5. Isolation of 1–3

The organic extract of *P. militaris* (4.06 g) was partitioned between 150 mL hexane and 150 mL 90% ACN three times. The pooled MeOH fractions were dried under reduced pressure and redissolved in 18 mL ACN. Aliquots of the sample were repeatedly injected onto a SUNFIRE column and eluted with a mobile phase consisting of solvents A (MQ-water and 0.1% formic acid) and B (acetonitrile and 0.1% formic acid), delivered in a gradient mode at 6 mL/min, starting from B at 10% to 58% over 16 min. The compounds

were collected with retention times of **1**: 13.6 min, **2**: 13.2 min and **3**: 12.9 min. Final separation of the compounds from sample impurities and each other were achieved by an extensive series of isolation steps. Aliquots of **1**, dried and dissolved in ACN, were injected onto a phenyl-hexyl column. Compound **1** eluted after 5.4 min (gradient: 24–51.5% B over 8 min).

3.6. Spectroscopic Data for the Isolated Compounds

3.6.1. Purpuroine K (**1**)

Light yellow wax; $[\alpha]_D^{20} + 13.63$ (c 0.22, MeOH); ^1H and ^{13}C NMR data, see Tables 1 and 2; HRESIMS m/z 486.8996 $[\text{M} + \text{H}]^+$ (Calcd for $\text{C}_{14}\text{H}_{20}^{79}\text{Br}_3\text{NO}_3$, 486.8993).

3.6.2. Purpuroine L (**2**)

Light brown wax; $[\alpha]_D^{20} 0.00$ (c 0.1, MeOH); ^1H and ^{13}C NMR data, see Tables 1 and 2; HRESIMS m/z 442.9414 $[\text{M} + \text{H}]^+$ (Calcd for $\text{C}_{14}\text{H}_{20}^{79}\text{Br}_2^{35}\text{ClNO}_3$, 442.9499).

3.6.3. Purpuroine M (**3**)

Light brown wax; $[\alpha]_D^{20} 0.00$ (c 0.05, MeOH); ^1H and ^{13}C NMR data, see Tables 1 and 2; HRESIMS m/z 398.9923 $[\text{M} + \text{H}]^+$ (Calcd for $\text{C}_{14}\text{H}_{20}^{79}\text{Br}^{35}\text{Cl}_2\text{NO}_3$, 399.0004).

3.7. Antibacterial and Biofilm Formation Inhibiting Activity of **1–3**

The three compounds (**1–3**) were tested for growth inhibiting abilities against five pathogenic bacterial strains. For the assay, *Staphylococcus aureus* (ATCC 25923), *Escherichia coli* (ATCC 25922) and *Pseudomonas aeruginosa* (ATCC 27853) were grown in Mueller Hinton broth (275730, Becton Dickinson and Company, Franklin Lakes, NJ, USA), and *Enterococcus faecalis* (ATCC 29212) and *Streptococcus agalactiae* (ATCC 12386) were grown in Brain Heart Infusion broth (53286, Sigma-Aldrich, St. Louis, MO, USA). The bacteria were grown on blood agar plates (University Hospital of North Norway, Tromsø, Norway) and a fresh colony was transferred to the appropriate growth media for an overnight incubation at 37 °C. The bacteria were diluted in fresh media to obtain exponential growth and reach a turbidity of 0.5 McFarland standard and added to a 96-well microtiter plate (734-2097, Nunclon™ Delta Surface, Thermo Scientific, Waltham, MA, USA). The total volume was 100 μL /well with 1500–15,000 CFU/well. The purpuroines were dissolved in Milli-Q water with 1% dimethyl sulfoxide (D4540, Sigma-Aldrich) and added to the wells in triplicates with a final concentration of 150 μM . The plate was incubated overnight at 37 °C, and the growth inhibition was measured with absorbance at 600 nm with 1420 Multilabel Counter VICTOR3™. Positive control for the assay was bacterial suspension with sterilised water (1:1) and negative control was sterilised water with growth media (1:1). A dilution series of gentamycin (A2712, Merck, Kenilworth, NJ, USA) from 32 to 0.01 $\mu\text{g}/\text{mL}$ was used as a reference control for the assay.

The biofilm formation inhibiting activity of compounds **1–3** against *Staphylococcus epidermidis* (ATCC 35984) was also investigated. *S. epidermidis* was grown on blood agar (University Hospital of North Norway, Tromsø, Norway) and one colony was transferred to Tryptic Soy Broth (22092, Sigma Aldrich) for overnight cultivation. The bacteria were diluted 1:100 in fresh medium with 1% dextrose (D9434, Sigma-Aldrich) to induce biofilm formation, before transferring to a 96-well Nunclon™ microtiter plate (50 μL /well). The compounds were added to the plate in triplicates, 50 μL /well giving a final volume of 100 μL /well. The purpuroines were dissolved in the same way as in the Growth Inhibition Assay and the test concentration was 150 μM for all the compounds. The plate was incubated overnight at 37 °C, and the bacteria were removed from the plate and the plate rinsed with tapped water. Before removing the bacteria, a visual examination of the plate was performed to exclude growth inhibition in any of the wells with the compounds. The biofilm formation was determined by staining with crystal violet (115940, Merck Millipore, Dramstadt, Germany). The biofilm was firstly fixated at 55 °C for one h before the biofilm was stained with 70 μL 0.1% crystal violet solution for 10 min. After incubation with crystal

violet the solution was again removed, and the plate was dried for one hour at 55 °C. When the plate was dry, 70 µL of 70% ethanol (ethanol 96%, 20823.362, VWR international, Radnor, PA, USA) was added to each well and the plate was incubated with shaking for 10 min. After incubation, the presence of biofilm was measured with absorbance at 600 nm with 1420 Multilabel Counter VICTOR3™. The positive control was bacterial suspension of *S. epidermidis* with sterilised water (1:1), and the negative control was bacterial suspension of a non-biofilm forming *Staphylococcus haemolyticus* (clinical isolate 8-7A, University Hospital of North Norway, Tromsø, Norway) with sterilised water (1:1). *S. haemolyticus* was also grown in TSB with 1% dextrose and treated in the same way as *S. epidermidis*. A medium blank was also prepared with TSB with 1% dextrose and sterilised water (1:1).

3.8. Antifungal Activity of 1–3

The yeast strains *Candida albicans* (ATCC 10231) and *Rhodotrula* sp. and the *Aurobasidium pollulans* mold, were cultivated on potato dextrose agar with 2% glucose at room temperature. Fungal spores were dissolved in potato dextrose broth (Difco Laboratories, USA) and the cell concentration was determined and adjusted after counting in a Bürker chamber. A final fungal spore concentration of 2×10^5 spores/mL were inoculated in 96-well nunc™ microtiter (100 µL total well volume) plates with a final assay concentration of 150 µM of compounds 1–3. The assay plates were incubated in a moist dark chamber at 37 °C. Ranging concentrations of amphotericin-B were used as positive control (MIC found to be 8.7 µM against all strains). Growth inhibition was determined microscopically after 42 h incubation.

3.9. Viability Screening

All cell lines were purchased from ATCC (Manassa, VA, USA) except MOLM-13 that was purchased from Leibniz Institute DSMZ (Braunschweig, Germany). Viability screening of compounds 1–3 at 10 and 50 µM was performed by a colorimetric MTS assay. The cells were seeded into 96-well microtiter plates (Nunclon™ Delta Surface, Thermo Scientific, Roskilde, Denmark) in RPMI-1640 supplemented with 10% FBS and 10 µg/mL Gentamycin (assay media). The adherent cell lines A2058, HaCat and HT29 were seeded in a density of 2000 cells/well, MRC5 were seeded in a density of 4000 cells/well and SK-BR-3 and MDA-MB-468 were seeded in a density of 5000 cells/well. After incubation for 24 h in 37 °C and 5% CO₂ the media was discarded and replaced by samples diluted in assay media, negative control (100% cell survival, 100% assay media) and positive control (0% cell survival, 90% assay media supplemented with 10% DMSO). The suspension cell lines MV-4-11 and MOLT-4 were directly seeded in a density of 10,000 cells/well and MOLM-13 and THP-1 were seeded in a density of 20,000 cells/well in assay media supplemented with sample. All samples were added in triplicates. Cells and samples were incubated for a total of 72 h (HepG2 cells were incubated for 24 h) at 37 °C and 5% CO₂. Thereafter, 10% CellTiter 96® AQueous One Solution Reagent (G3581, Promega) containing tetrazolium compound [3-(4,5-dimethylthiazol-2-yl)-5-(3-carboxymethoxyphenyl)-2-(4-sulfophenyl)-2H-tetrazolium] and phenazine ethosulfate were added. After 1 h incubation the absorbances was measured at 485 nm with a DTX 880 and viability was calculated.

3.10. Cell Cycle Analysis

MV-4-11 cells were seeded into 24-well plates (Nunclon™ Delta Surface, Thermo Scientific) in a density of 1×10^6 cells/mL supplemented with 26 µM, 52 µM or 104 µM of 1. The cells were incubated for 24 h and thereafter fixed in ice cold 70% EtOH. After washing the cells were stained with FxCycle™ PI/RNase Staining Solution (Invitrogen, MA, USA) according to manufacturer's instructions. The cells were analysed by a CytoFLEX Flow cytometer (Beckman Coulter, CA, USA) and cell cycle phase determined in CytExpert software (Beckman Coulter).

3.11. Apoptosis Assay

MV-4-11 cells were seeded into 24-well plates (Nunclon™ Delta Surface, Thermo Scientific) at a density of 1×10^6 cells/mL supplemented with 26 μ M, 52 μ M or 104 μ M of **1** and incubated for 24 or 48 h at 37 °C an 5% CO₂. Apoptotic and necrotic cells were labelled according to manufacturer's instructions (Alexa Fluor™ 488 Annexin V/Dead Cell Apoptosis Kit, Invitrogen) and analysed by a CytoFLEX Flow cytometer and CytExpert software (Beckman Coulter).

3.12. Kinase Binding Assay

The FLT3 variants (FLT WT: catalogue number PV3182, lot number 2180555F; FLT ITD: catalogue number PV6191, lot number 2395171), Eu-anti-His tag antibody (catalogue number PV5596), and fluorescent tracer 236 (catalogue number PV5592) were purchased from ThermoFisher Scientific (Oslo, Norway). Anti-GST-Eu-tagged monoclonal antibodies (anti-GST AB) were purchase from Cisbio (PerkinElmer Norge AS, catalogue number 61GSTKLA) and reconstituted in water at a final concentration of 333 nM. White, non-binding, round bottom 384 well microplates (reference number 4513) were purchased from Corning (Corning Inc., Kennebunk, ME, USA). The compounds were serially diluted into DMSO to 12 different concentrations. Each of these compound-containing DMSO solutions was further diluted 33 times in assay buffer A (50 mM HEPES pH 7.5, 10 mM MgCl₂, 1 mM ethylene glycol-bis(β -aminoethyl ether)-N,N,N',N'-tetraacetic acid (EGTA) and 0.01% BRIJ-35) and 5 μ L of these solutions were dispensed in triplicates in 384 well plate. FLT3 variants were mixed to their respective Eu tagged antibodies: FLT3 WT at 30 nM kinase concentration + 6 nM of anti- His AB and FLT3 ITD at 30 nM of kinase concentration + 12 nM of anti-GST AB. The tracer 236 was diluted to a concentration of 15 nM in buffer A. Finally, 5 μ L of the kinase + antibody solution and 5 μ L of the tracer solution were added to each of the wells containing 5 μ L of compound in the 384 microwell plate. The plate was shaken for 1 min at 1000 rpm and incubated in the dark at room temperature for 1 h. Fluorescence measurements were made using a EnVision 2104 Multilabel reader, (PerkinElmer, Waltham, MA, USA), excitation wavelength was set to 340 nm and emission was read at both 615 nm (8.5 nm bandwidth) and 665 nm (7.5 nm bandwidth) over 200 ms with a 100 ms delay between excitation and emission measurements. Emission ratio was calculated by dividing the signal at 665 nm by the signal at 615 nm for each compound and concentration. Emission ratios were normalised and plotted against the concentration and fitted with an inhibition curve (with Hill coefficient fixed to -1) of the form: $(Y = 100/(1 + (X/IC_{50}))$) to obtain the IC₅₀. Since compound **1** did not show binding to any of the FLT3 variants, the fitting of the results using this equation was poor and we decided to not display the fitting curve for compound **1** on Figure 6.

3.13. Docking Studies

The compounds were imported into the Maestro Suite release 2022-2 (Maestro version 13.2.128, Schrödinger LLC, New York, NY, USA) as SMILES and prepared with LigPrep, using EPIK to simulate the protonation and tautomerisation states at pH 7.4 ± 3.0 [39,40]. After manual inspection, it was decided to use the model of the cytoplasmic kinase domain of FLT3 WT with PDB ID: 6JQR [35] for docking studies. The endogenous ligand was extracted from the protein model and prepared with LigPrep as described above. The protein model 6JQR without ligand was made ready for docking using the protein preparation wizard from Schrödinger (release 2022-2) [41]. Briefly hydrogen atoms were replaced, missing side chains and loops were repaired with PRIME [42], residues with multiple conformers were set to the conformers with the highest occupancy, all atoms were then minimised and finally water and solvent molecules were removed. A docking grid of approximate size $25 \text{ \AA} \times 25 \text{ \AA} \times 25 \text{ \AA}$ was generated around the active site of the prepared model, using the location of the endogenous ligand for centring. The prepared ligands were docked using GLIDE extra precision docking [36–38], allowing up to 3 poses per

ligand and without additional constraints. Results were inspected with Maestro, figures were produced with Maestro and ChimeraX [43].

4. Conclusions

In this paper we have identified three previously undescribed purpuroines analogues, purpuroine K–M (compound 1–3). The compounds did not show antifungal or antibacterial activity and did not inhibit biofilm formation. Interestingly, one of the analogues, purpuroine K (1), selectively inhibited the cancerous cell lines MV-4-11 and MOLM-13, two cellular models of FLT3-ITD positive human AML. Compound 1 caused cellular arrest in cell cycle phase G0/G1 and induced apoptosis in the MV-4-11 cells similar to other FLT3 inhibitors. Kinase binding and docking studies did not reveal strong binding of the compound to the FLT3 kinase and the complete mechanism behind its effects needs to be further studied. However, this indicates that it is possible to inhibit FLT3 driven AML cell lines without targeting the active site of FLT3.

Supplementary Materials: The supporting information can be downloaded at: <https://www.mdpi.com/article/10.3390/ijms232415852/s1>.

Author Contributions: Conceptualization, S.U., G.A.P. and K.Ø.H.; Data curation, S.U., G.A.P., J.I., M.J., C.L. and K.Ø.H.; Formal analysis, S.U. and G.A.P.; Investigation, S.U., G.A.P., J.I., M.J., C.L. and K.Ø.H.; Methodology, S.U., G.A.P., J.I. and K.Ø.H.; Project administration, K.Ø.H.; Resources, K.Ø.H.; Software, S.U.; Supervision, K.Ø.H.; Validation, S.U., G.A.P., J.I., I.K.Ø.H., Y.K.-H.S., M.J., C.L. and K.Ø.H.; Visualization, S.U. and K.Ø.H.; Writing—original draft, S.U., G.A.P. and K.Ø.H.; Writing—review and editing, S.U., G.A.P. and K.Ø.H. All authors have read and agreed to the published version of the manuscript.

Funding: This research received no external funding.

Institutional Review Board Statement: Not applicable.

Informed Consent Statement: Not applicable.

Data Availability Statement: Data available on request from the authors.

Acknowledgments: We are grateful to Marbank for collecting the specimens of *P. militaris* and to R. Johansen for taxonomic identification of the organism.

Conflicts of Interest: The authors declare no conflict of interest.

References

1. Hu, Y.; Chen, J.; Hu, G.; Yu, J.; Zhu, X.; Lin, Y.; Chen, S.; Yuan, J. Statistical Research on the Bioactivity of New Marine Natural Products Discovered during the 28 Years from 1985 to 2012. *Mar. Drugs* **2015**, *13*, 202. [CrossRef] [PubMed]
2. Newman, D.J.; Cragg, G.M. Natural Products as Sources of New Drugs from 1981 to 2014. *J. Nat. Prod.* **2016**, *79*, 629–661. [CrossRef]
3. Blunt, J.W.; Carroll, A.R.; Copp, B.R.; Davis, R.A.; Keyzers, R.A.; Prinsep, M.R. Marine natural products. *Nat. Prod. Rep.* **2018**, *35*, 8–53. [CrossRef]
4. Bell, M.V.; Sargent, J.R. Fatty acid compositions of neutral glycerides from the ovaries of the asteroids *Ctenodiscus crispatus*, *Asterias lincki* and *Pteraster militaris* from Balsfjorden, northern Norway. *J. Exp. Mar. Biol. Ecol.* **1985**, *87*, 31–40. [CrossRef]
5. Albrizio, S.; Ciminiello, P.; Fattorusso, E.; Magno, S.; Pansini, M. Chemistry of Verongida sponges. I. Constituents of the Caribbean sponge *Pseudoceratina crassa*. *Tetrahedron* **1994**, *50*, 783–788. [CrossRef]
6. Shen, S.; Liu, D.; Wei, C.; Proksch, P.; Lin, W. Purpuroines A–J, halogenated alkaloids from the sponge *Iotrochota purpurea* with antibiotic activity and regulation of tyrosine kinases. *Bioorg. Med. Chem.* **2012**, *20*, 6924–6928. [CrossRef]
7. Tsuda, M.; Endo, T.; Watanabe, K.; Fromont, J.; Kobayashi, J. Nakirodin A, a bromotyrosine alkaloid from a Verongid sponge. *J. Nat. Prod.* **2002**, *65*, 1670–1671. [CrossRef]
8. Jurek, J.; Yoshida, W.Y.; Scheuer, P.J.; Kelly-Borges, M. Three new bromotyrosine-derived metabolites of the sponge *Psammaolysilla purpurea*. *J. Nat. Prod.* **1993**, *56*, 1609–1612. [CrossRef]
9. Gao, H.; Kelly, M.; Hamann, M.T. Bromotyrosine-derived metabolites from the sponge *Aiolochoira crassa*. *Tetrahedron* **1999**, *55*, 9717–9726. [CrossRef]
10. Galeano, E.; Thomas, O.P.; Robledo, S.; Munoz, D.; Martinez, A. Antiparasitic bromotyrosine derivatives from the marine sponge *Verongula rigida*. *Mar. Drugs* **2011**, *9*, 1902–1913. [CrossRef] [PubMed]

11. Ciminiello, P.; Fattorusso, E.; Magno, S.; Pansini, M. Chemistry of Verongida Sponges, III. Constituents of a Caribbean *Verongula* sp. *J. Nat. Prod.* **1994**, *57*, 1564–1569. [[CrossRef](#)]
12. Ciminiello, P.; Fattorusso, E.; Magno, S.; Pansini, M. Chemistry of Verongida Sponges, IV. Comparison of the secondary metabolite composition of several specimens of *Pseudoceratina crassa*. *J. Nat. Prod.* **1995**, *58*, 689–696. [[CrossRef](#)]
13. Kazi, J.U.; Rönnstrand, L. FMS-like Tyrosine Kinase 3/FLT3: From Basic Science to Clinical Implications. *Physiol. Rev.* **2019**, *99*, 1433–1466. [[CrossRef](#)]
14. Meshinchi, S.; Appelbaum, F.R. Structural and functional alterations of FLT3 in acute myeloid leukemia. *Clin. Cancer. Res.* **2009**, *15*, 4263–4269. [[CrossRef](#)]
15. Griffith, J.; Black, J.; Faerman, C.; Swenson, L.; Wynn, M.; Lu, F.; Lippke, J.; Saxena, K. The Structural Basis for Autoinhibition of FLT3 by the Juxtamembrane Domain. *Mol. Cell* **2004**, *13*, 169–178. [[CrossRef](#)]
16. Verstraete, K.; Vandriessche, G.; Januar, M.; Elegheert, J.; Shkumatov, A.V.; Desfosses, A.; Van Craenenbroeck, K.; Svergun, D.I.; Gutsche, I.; Vergauwen, B. Structural insights into the extracellular assembly of the hematopoietic Flt3 signaling complex. *Blood* **2011**, *118*, 60–68. [[CrossRef](#)]
17. Grafone, T.; Palmisano, M.; Nicci, C.; Storti, S. An overview on the role of FLT3-tyrosine kinase receptor in acute myeloid leukemia: Biology and treatment. *Oncol. Rev.* **2012**, *6*, e8. [[CrossRef](#)] [[PubMed](#)]
18. Stirewalt, D.L.; Radich, J.P. The role of FLT3 in haematopoietic malignancies. *Nat. Rev. Cancer* **2003**, *3*, 650–665. [[CrossRef](#)] [[PubMed](#)]
19. Kiyoi, H.; Kawashima, N.; Ishikawa, Y. FLT3 mutations in acute myeloid leukemia: Therapeutic paradigm beyond inhibitor development. *Cancer Sci.* **2020**, *111*, 312–322. [[CrossRef](#)] [[PubMed](#)]
20. Kennedy, V.E.; Smith, C.C. FLT3 Mutations in Acute Myeloid Leukemia: Key Concepts and Emerging Controversies. *Front. Oncol.* **2020**, *10*, 612880. [[CrossRef](#)]
21. Wu, W.J.; Wu, Y.K.; Liu, B. Synthesis of purpuroine A, nakirodin A and MDN-0104: The hidden puzzles and risk of error in their configurational assignments. *Tetrahedron* **2017**, *73*, 1265–1274. [[CrossRef](#)]
22. Paul, V.J.; Pennings, S.C. Diet-derived chemical defenses in the sea hare *Stylocheilus longicauda* (Quoy et Gaimard 1824). *J. Exp. Mar. Biol. Ecol.* **1991**, *151*, 227–243. [[CrossRef](#)]
23. Rossini, C.; Bezzerides, A.; González, A.; Eisner, M.; Eisner, T. Chemical defense: Incorporation of diet-derived pyrrolizidine alkaloid into the integumental scales of a moth (*Utetheisa ornatrix*). *Chemoecology* **2003**, *13*, 199–205. [[CrossRef](#)]
24. Mah, C.L.; Blake, D.B. Global diversity and phylogeny of the Asteroidea (Echinodermata). *PLoS ONE* **2012**, *7*, e35644. [[CrossRef](#)]
25. Mauzey, K.P.; Birkeland, C.; Dayton, P.K. Feeding Behavior of Asteroids and Escape Responses of their Prey in the Puget Sound Region. *Ecology* **1968**, *49*, 603–619. [[CrossRef](#)]
26. Lagunas-Rangel, F.A.; Chavez-Valencia, V. FLT3-ITD and its current role in acute myeloid leukaemia. *Med. Oncol.* **2017**, *34*, 114. [[CrossRef](#)]
27. Bailon-Moscoso, N.; Cevallos-Solorzano, G.; Romero-Benavides, J.C.; Orellana, M.I. Natural Compounds as Modulators of Cell Cycle Arrest: Application for Anticancer Chemotherapies. *Curr. Genom.* **2017**, *18*, 106–131. [[CrossRef](#)]
28. Wang, L.; Wang, J.; Blaser, B.W.; Duchemin, A.M.; Kusewitt, D.F.; Liu, T.; Caligiuri, M.A.; Briesewitz, R. Pharmacologic inhibition of CDK4/6: Mechanistic evidence for selective activity or acquired resistance in acute myeloid leukemia. *Blood* **2007**, *110*, 2075–2083. [[CrossRef](#)]
29. Sexauer, A.; Perl, A.; Yang, X.; Borowitz, M.; Gocke, C.; Rajkhowa, T.; Thiede, C.; Frattini, M.; Nybakken, G.E.; Pratz, K.; et al. Terminal myeloid differentiation in vivo is induced by FLT3 inhibition in FLT3/ITD AML. *Blood* **2012**, *120*, 4205–4214. [[CrossRef](#)]
30. Eriksson, A.; Kalushkova, A.; Jarvius, M.; Hillhorst, R.; Rickardson, L.; Kultima, H.G.; de Wijn, R.; Hovestad, L.; Fryknas, M.; Oberg, F.; et al. AKN-028 induces cell cycle arrest, downregulation of Myc associated genes and dose dependent reduction of tyrosine kinase activity in acute myeloid leukemia. *Biochem. Pharmacol.* **2014**, *87*, 284–291. [[CrossRef](#)]
31. Guo, Y.; Chen, Y.; Xu, X.; Fu, X.; Zhao, Z.J. SU11652 Inhibits tyrosine kinase activity of FLT3 and growth of MV-4-11 cells. *J. Hematol. Oncol.* **2012**, *5*, 72. [[CrossRef](#)]
32. Wu, M.; Zhu, X. FLT3 inhibitors in acute myeloid leukemia. *J. Hematol. Oncol.* **2018**, *11*, 133. [[CrossRef](#)] [[PubMed](#)]
33. Zhu, R.; Li, L.; Nguyen, B.; Seo, J.; Wu, M.; Seale, T.; Levis, M.; Duffield, A.; Hu, Y.; Small, D. FLT3 tyrosine kinase inhibitors synergize with BCL-2 inhibition to eliminate FLT3/ITD acute leukemia cells through BIM activation. *Signal Transduct. Target. Ther.* **2021**, *6*, 186. [[CrossRef](#)] [[PubMed](#)]
34. Gu, J.; Gui, Y.; Chen, L.; Yuan, G.; Lu, H.Z.; Xu, X. Use of natural products as chemical library for drug discovery and network pharmacology. *PLoS ONE* **2013**, *8*, e62839. [[CrossRef](#)] [[PubMed](#)]
35. Kawase, T.; Nakazawa, T.; Eguchi, T.; Tsuzuki, H.; Ueno, Y.; Amano, Y.; Suzuki, T.; Mori, M.; Yoshida, T. Effect of Fms-like tyrosine kinase 3 (FLT3) ligand (FL) on antitumor activity of gilteritinib, a FLT3 inhibitor, in mice xenografted with FL-overexpressing cells. *Oncotarget* **2019**, *10*, 6111–6123. [[CrossRef](#)] [[PubMed](#)]
36. Friesner, R.A.; Murphy, R.B.; Repasky, M.P.; Frye, L.L.; Greenwood, J.R.; Halgren, T.A.; Sanschagrin, P.C.; Mainz, D.T. Extra Precision Glide: Docking and Scoring Incorporating a Model of Hydrophobic Enclosure for Protein–Ligand Complexes. *J. Med. Chem.* **2006**, *49*, 6177–6196. [[CrossRef](#)] [[PubMed](#)]
37. Halgren, T.A.; Murphy, R.B.; Friesner, R.A.; Beard, H.S.; Frye, L.L.; Pollard, W.T.; Banks, J.L. Glide: A new approach for rapid, accurate docking and scoring. 2. Enrichment factors in database screening. *J. Med. Chem.* **2004**, *47*, 1750–1759. [[CrossRef](#)]

38. Friesner, R.A.; Banks, J.L.; Murphy, R.B.; Halgren, T.A.; Klicic, J.J.; Mainz, D.T.; Repasky, M.P.; Knoll, E.H.; Shelley, M.; Perry, J.K.; et al. Glide: A new approach for rapid, accurate docking and scoring. 1. Method and assessment of docking accuracy. *J. Med. Chem.* **2004**, *47*, 1739–1749. [[CrossRef](#)] [[PubMed](#)]
39. Greenwood, J.R.; Calkins, D.; Sullivan, A.P.; Shelley, J.C. Towards the comprehensive, rapid, and accurate prediction of the favorable tautomeric states of drug-like molecules in aqueous solution. *J. Comput.-Aided Mol. Des.* **2010**, *24*, 591–604. [[CrossRef](#)] [[PubMed](#)]
40. Shelley, J.C.; Cholleti, A.; Frye, L.L.; Greenwood, J.R.; Timlin, M.R.; Uchimaya, M. Epik: A software program for pK_a prediction and protonation state generation for drug-like molecules. *J. Comput.-Aided Mol. Des.* **2007**, *21*, 681–691. [[CrossRef](#)]
41. Madhavi Sastry, G.; Adzhigirey, M.; Day, T.; Annabhimoju, R.; Sherman, W. Protein and ligand preparation: Parameters, protocols, and influence on virtual screening enrichments. *J. Comput.-Aided Mol. Des.* **2013**, *27*, 221–234. [[CrossRef](#)] [[PubMed](#)]
42. Jacobson, M.P.; Pincus, D.L.; Rapp, C.S.; Day, T.J.; Honig, B.; Shaw, D.E.; Friesner, R.A. A hierarchical approach to all-atom protein loop prediction. *Proteins* **2004**, *55*, 351–367. [[CrossRef](#)] [[PubMed](#)]
43. Pettersen, E.F.; Goddard, T.D.; Huang, C.C.; Meng, E.C.; Couch, G.S.; Croll, T.I.; Morris, J.H.; Ferrin, T.E. UCSF ChimeraX: Structure visualization for researchers, educators, and developers. *Protein Sci.* **2021**, *30*, 70–82. [[CrossRef](#)] [[PubMed](#)]